

The mean shape of transition and first-passage paths

Won Kyu Kim* and Roland R. Netz†
*Department of Physics, Freie Universität Berlin,
Arnimallee 14, 14195 Berlin, Germany*

We calculate the mean shape of transition paths and first-passage paths based on the one-dimensional Fokker-Planck equation in an arbitrary free energy landscape including a general inhomogeneous diffusivity profile. The transition path ensemble is the collection of all paths that do not revisit the start position x_A and that terminate when first reaching the final position x_B . In contrast, a first-passage path can revisit but not cross its start position x_A before it terminates at x_B . Our theoretical framework employs the forward and backward Fokker-Planck equations as well as first-passage, passage, last-passage and transition-path time distributions, for which we derive the defining integral equations. We show that the mean time at which the transition path ensemble visits an intermediate position x is equivalent to the mean first-passage time of reaching the starting position x_A from x without ever visiting x_B . The mean shape of first-passage paths is related to the mean shape of transition paths by a constant time shift. Since for large barrier height U the mean first-passage time scales exponentially in U while the mean transition path time scales linearly inversely in U , the time shift between first-passage and transition path shapes is substantial. We present explicit examples of transition path shapes for linear and harmonic potentials and illustrate our findings by trajectories generated from Brownian dynamics simulations.

I. INTRODUCTION

For a reaction involving a free energetic barrier, the ensemble of transition paths is the collection of all paths that lead from the reactant to the product ensemble without recrossing the boundaries between the transition domain and the reactant domains [1–3]. For continuous paths described by the Fokker-Planck equation, transition paths can be generated by imposing absorbing boundary conditions on the boundaries between the reactant, transition and product domains [4]. The mean transition path time τ^{TP} is the first moment of the transition path time distribution. Based on an explicit formula derived by A. Szabo for the one-dimensional case [4], τ^{TP} is for a large free-energetic barrier U much shorter than Kramers' mean first-passage time τ^{KFP} . Note that a first-passage path is allowed to revisit its origin many times and in the Fokker-Planck description is obtained by imposing a reflecting boundary condition at the start position. In fact, while Kramers' mean first-passage time grows exponentially with the energy barrier height U , the mean transition path time decreases linearly inversely in U for a fixed separation between the start and final position along the one-dimensional reaction coordinate [5]. This means that in a reaction involving a large energetic barrier, the system spends an exponential amount of time revisiting the reactant state, while the actual transition occurs very quickly [6, 7].

Although transition paths are crucial for the understanding of rare events, they are in typical experiments that measure reaction rates not directly accessible. This

situation dramatically changed with the advent of high resolution single molecule experiments that allow to actually observe the folding and unfolding transition paths of proteins [6–10] as well as nucleic acid molecules [11–13]. Note that in these experiments, reaction paths are typically obtained from the FRET efficiency between fluorophores connected to molecular positions that allow to separate folded from unfolded state. As such, these experiments project the complex molecular dynamics onto a one-dimensional reaction coordinate that corresponds to an intramolecular distance, which motivated extensive theoretical work using models restricted to one-dimensional diffusion (though it is clear that a projection into one dimension does not necessarily mean that a Markovian description is valid). Indeed, in these experiments it was found that the mean transition path time is significantly smaller than the folding or unfolding time. In fact, the transition typically occurs so quickly that only upper estimates can experimentally be obtained, which from early estimates of about $\tau^{TP} < 200 \mu\text{s}$ for proteins as well as RNA [6, 7, 11], has come down to $\tau^{TP} < 10 \mu\text{s}$ with improved experimental time resolution [8–10, 12].

The experimental advances created theoretical interest in transition paths and led to intense simulation activities [14–16] as well as the development of analytic approaches [5, 17, 18]. In this work, we present a theoretical framework for transition paths involving a combination of the backward Fokker-Planck equation, the forward Fokker-Planck equation, and the renewal equation approach, and use it to derive the mean shape of transition paths. We use the same framework to also calculate the mean shape of Kramers' first-passage paths. Interestingly, first-passage and transition path shapes are identical modulo a shift by constant time which correspond to the residence time at the start position and is given by

*Electronic address: wkkim@physik.fu-berlin.de

†Electronic address: rnetz@physik.fu-berlin.de

the difference of Kramers' mean first-passage time and the mean transition path time. We present explicit results for transition path shapes for constant, linear and harmonic potentials and illustrate our findings with transition and first-passage paths generated using Brownian dynamics simulations.

II. DERIVATION OF TRANSITION PATH TIMES AND SHAPES

The Fokker-Planck (FP) operator is defined as [19–21]

$$\mathcal{L}(x) = \partial_x D(x) e^{-F(x)} \partial_x e^{F(x)}, \quad (1)$$

where $F(x)$ is the free energy in units of the thermal energy $k_B T$ and $D(x)$ is the position-dependent diffusivity. In our previous analysis of protein folding trajectories from molecular dynamics trajectories we found that the diffusivity profile has a pronounced spatial dependence, together with the free energy profile it allows to predict kinetics that is rather insensitive on the precise definition of the reaction coordinate [22]. But even for the much simpler system of two water molecules diffusing relative to each other the diffusivity profile is not constant and therefore is important to take into account [23]. The Green's function can be formally written as

$$\mathcal{G}(x, t|x_0) = e^{t\mathcal{L}(x)} \delta(x - x_0). \quad (2)$$

It fulfills the initial condition

$$\mathcal{G}(x, 0|x_0) = \delta(x - x_0), \quad (3)$$

and solves the forward FP equation

$$\partial_t \mathcal{G}(x, t|x_0) = \mathcal{L}(x) \mathcal{G}(x, t|x_0). \quad (4)$$

The adjoint FP operator [19–21]

$$\mathcal{L}^\dagger(x_0) = e^{F(x_0)} \partial_{x_0} D(x_0) e^{-F(x_0)} \partial_{x_0}, \quad (5)$$

solves the backward FP equation

$$\partial_t \mathcal{G}(x, t|x_0) = \mathcal{L}^\dagger(x_0) \mathcal{G}(x, t|x_0). \quad (6)$$

We will in the following section first use the backward FP equation, as it allows to derive transition path times and first-passage times in a most transparent and direct fashion. We will then use the forward FP approach, which requires careful normalization of expectation values but allows to calculate mean passage times and from that various relations between mean transition path, first-passage and passage times. Finally, we use the renewal equation approach to derive constitutive relations between transition path time, first-passage time and last-passage time distributions. Here we will be able to present a clear interpretation of the expression derived for the mean shape of transition and first-passage paths.

A. Backward Fokker-Planck approach

1. First-passage time distributions

The derivation in this section uses concepts and techniques presented previously in [20, 21]. By assuming absorbing boundary conditions at positions x_A and x_B we calculate first-passage times for paths that start at x_0 with $x_A < x_0 < x_B$ and reach the boundaries for the first time. For this we define the survival probability

$$S(x_0, t) = \int_{x_A}^{x_B} dx \mathcal{G}(x, t|x_0), \quad (7)$$

that the paths have not reached yet an absorbing boundary with the obvious properties $S(x_0, 0) = 1$ and, for regular free energies, $S(x_0, \infty) = 0$. The first-passage distribution for reaching either one of the boundaries is defined as

$$K(x_A \vee x_B, t|x_0) = -\partial_t S(x_0, t), \quad (8)$$

and by using Eq. (4) can be rewritten as

$$\begin{aligned} K(x_A \vee x_B, t|x_0) &= -\int_{x_A}^{x_B} dx \mathcal{L}(x) \mathcal{G}(x, t|x_0) \\ &= \int_{x_A}^{x_B} dx \partial_x j(x, t|x_0) \\ &= j(x_B, t|x_0) - j(x_A, t|x_0), \end{aligned} \quad (9)$$

where we used the flux at position x defined as

$$j(x, t|x_0) = -D(x) e^{-F(x)} \partial_x e^{F(x)} \mathcal{G}(x, t|x_0). \quad (10)$$

This shows that the total first-passage distribution can be decomposed into the two first-passage distributions $K(x_A, t|x_0) = -j(x_A, t|x_0)$ and $K(x_B, t|x_0) = j(x_B, t|x_0)$ corresponding to the respective boundary fluxes according to

$$K(x_A \vee x_B, t|x_0) = K(x_A, t|x_0) + K(x_B, t|x_0). \quad (11)$$

By applying the flux operator defined in Eq. (10) on both sides of the backward FP equation Eq. (6) we obtain explicit equations for the first-passage distributions $K(x_A, t|x_0)$ and $K(x_B, t|x_0)$ as

$$\partial_t K(x_{A/B}, t|x_0) = \mathcal{L}^\dagger(x_0) K(x_{A/B}, t|x_0). \quad (12)$$

Defining the n -th moments of the first-passage distributions as

$$K^{(n)}(x_{A/B}|x_0) = \int_0^\infty dt t^n K(x_{A/B}, t|x_0), \quad (13)$$

we obtain from Eq. (12) the set of equations

$$-nK^{(n-1)}(x_{A/B}|x_0) = \mathcal{L}^\dagger(x_0) K^{(n)}(x_{A/B}|x_0), \quad (14)$$

where in the derivation we used the boundary condition that $K(x_{A/B}, t|x_0) = 0$ for $t = 0$ and $t = \infty$. Thus

all moments can be calculated recursively by straightforward integration of Eq. (14). The zeroth moment of the first-passage distribution is nothing but the splitting probability,

$$\phi_{A/B}(x_0) = K^{(0)}(x_{A/B}|x_0), \quad (15)$$

which gives the probability that a path starting at x_0 reaches the boundary at x_A or x_B . From Eq. (14) we obtain for $n = 0$

$$\mathcal{L}^\dagger(x_0)\phi_{A/B}(x_0) = 0. \quad (16)$$

From Eq. (8) and the boundary conditions $S(x_0, 0) = 1$ and $S(x_0, \infty) = 0$ we conclude that $\int_0^\infty dt [K(x_A, t|x_0) + K(x_B, t|x_0)] = 1$, in other words, the sum of the splitting probabilities is unity, eventually the path reaches a boundary,

$$\phi_A(x_0) + \phi_B(x_0) = 1. \quad (17)$$

For $n = 1$ we obtain from Eq. (14)

$$\mathcal{L}^\dagger(x_0)K^{(1)}(x_{A/B}|x_0) = -\phi_{A/B}(x_0). \quad (18)$$

Since the first-passage distributions $K^{(1)}(x_A|x_0)$ and $K^{(1)}(x_B|x_0)$ are not normalized, reflected by the fact that the splitting probabilities $\phi_{A/B}(x_0)$ are smaller than unity, the mean first-passage times are after normalization given by

$$\tau^{FP}(x_{A/B}|x_0) = \frac{K^{(1)}(x_{A/B}|x_0)}{\phi_{A/B}(x_0)}. \quad (19)$$

As a side remark, the mean first-passage time to reach either the boundary x_A or x_B is given by the sum of the first moments $\tau^{FP}(x_A \vee x_B|x_0) = K^{(1)}(x_A|x_0) + K^{(1)}(x_B|x_0)$. Adding the two equations for $K^{(1)}(x_A|x_0)$ and $K^{(1)}(x_B|x_0)$ in Eq. (18) and using that $\phi_A(x_0) + \phi_B(x_0) = 1$ we arrive at the familiar equation [20, 21]

$$\mathcal{L}^\dagger(x_0)\tau^{FP}(x_A \vee x_B|x_0) = -1. \quad (20)$$

2. Splitting probabilities

We explicitly show the calculation of the splitting probabilities, all further calculations proceed similarly and are

not detailed. We write Eq. (16) explicitly for $\phi_B(x_0)$,

$$e^{F(x_0)}\partial_{x_0}D(x_0)e^{-F(x_0)}\partial_{x_0}\phi_B(x_0) = 0. \quad (21)$$

Integrating once we obtain

$$\frac{e^{F(x)}}{D(x)} = C\partial_x\phi_B(x), \quad (22)$$

where C is an integration constant that will be determined later. Another integration yields

$$C^{-1} \int_{x_A}^{x_0} dx \frac{e^{F(x)}}{D(x)} = \phi_B(x)|_{x_A}^{x_0} = \phi_B(x_0), \quad (23)$$

where we used that $\phi_B(x_A) = 0$, i.e., a path that starts at the absorbing boundary at x_A will be immediately absorbed and the probability to reach x_B vanishes. Conversely, $\phi_B(x_B) = 1$ and thus

$$C = \int_{x_A}^{x_B} dx \frac{e^{F(x)}}{D(x)}. \quad (24)$$

For $\phi_A(x_0)$ we obtain

$$\phi_A(x_0) = 1 - \phi_B(x_0) = \frac{1}{C} \int_{x_0}^{x_B} dx \frac{e^{F(x)}}{D(x)}. \quad (25)$$

3. Mean first-passage times

From Eq. (18) and using the results for $\phi_A(x_0)$ and $\phi_B(x_0)$ in Eqs. (23) and (25) we can straightforwardly calculate the first moments of the first-passage distributions. The boundary conditions require some thought: The mean first-passage time to reach either absorbing boundary, $\tau^{FP}(x_A \vee x_B|x_0) = K^{(1)}(x_A|x_0) + K^{(1)}(x_B|x_0)$, vanishes at the boundaries, i.e., $\tau^{FP}(x_A \vee x_B|x_A) = \tau^{FP}(x_A \vee x_B|x_B) = 0$. It follows that both first moments $K^{(1)}(x_A|x_0)$ and $K^{(1)}(x_B|x_0)$ must individually vanish at the absorbing boundaries, i.e. $K^{(1)}(x_A|x_A) = K^{(1)}(x_A|x_B) = 0$ and $K^{(1)}(x_B|x_A) = K^{(1)}(x_B|x_B) = 0$. With these boundary conditions we obtain

$$K^{(1)}(x_A|x_0) = C\phi_B(x_0) \int_{x_0}^{x_B} dx e^{-F(x)}\phi_A^2(x) + C\phi_A(x_0) \int_{x_A}^{x_0} dx e^{-F(x)}\phi_A(x)\phi_B(x), \quad (26)$$

and

$$K^{(1)}(x_B|x_0) = C\phi_A(x_0) \int_{x_A}^{x_0} dx e^{-F(x)}\phi_B^2(x) + C\phi_B(x_0) \int_{x_0}^{x_B} dx e^{-F(x)}\phi_A(x)\phi_B(x). \quad (27)$$

From Eq. (19) the mean first-passage time to reach boundary A when starting from x_0 reads

$$\tau^{FP}(x_A|x_0) = C \frac{\phi_B(x_0)}{\phi_A(x_0)} \int_{x_0}^{x_B} dx e^{-F(x)} \phi_A^2(x) + C \int_{x_A}^{x_0} dx e^{-F(x)} \phi_A(x) \phi_B(x), \quad (28)$$

while the mean first-passage time to reach boundary B when starting from x_0 reads

$$\tau^{FP}(x_B|x_0) = C \frac{\phi_A(x_0)}{\phi_B(x_0)} \int_{x_A}^{x_0} dx e^{-F(x)} \phi_B^2(x) + C \int_{x_0}^{x_B} dx e^{-F(x)} \phi_A(x) \phi_B(x). \quad (29)$$

As we will show explicitly below, because of reversibility, the mean first-passage time $\tau^{FP}(x_A|x_0)$ in fact equals the mean-time a transition path that starts at the boundary x_A and ends at the boundary x_B needs in order to reach the intermediate position x_0 , it thus determines the mean shape of the transition path,

$$\tau_{shape}^{TP}(x_0|x_A) = \tau^{FP}(x_A|x_0), \quad (30)$$

parameterized in terms of the mean time as a function of the position. Likewise, the mean first-passage time $\tau^{FP}(x_B|x_0)$ corresponds to the mean time a transition path that starts at boundary x_B and ends at boundary x_A needs in order to reach the intermediate position x_0 ,

$$\tau_{shape}^{TP}(x_0|x_B) = \tau^{FP}(x_B|x_0). \quad (31)$$

Note that the paths that contribute to the shape $\tau_{shape}^{TP}(x_0|x_{A/B})$ revisit the position x_0 multiple times, as will be illustrated later on when we present explicit Brownian dynamics paths.

4. Transition path times

The transition path time denotes the mean time a path takes to reach from the absorbing boundary x_A to the other absorbing boundary at x_B . It is thus defined by

$$\tau^{TP}(x_B|x_A) = \tau^{FP}(x_B|x_0 \rightarrow x_A). \quad (32)$$

In the limit $x_0 \rightarrow x_A$ the first term in Eq. (29) vanishes and we obtain in agreement with Szabo's result [4]

$$\tau^{TP}(x_B|x_A) = C \int_{x_A}^{x_B} dx e^{-F(x)} \phi_A(x) \phi_B(x). \quad (33)$$

The same result is obtained from Eq. (28) by the limiting procedure $\tau^{TP}(x_A|x_B) = \tau^{FP}(x_A|x_0 \rightarrow x_B)$, reflecting that transition paths are reversible, i.e. $\tau^{TP}(x_B|x_A) = \tau^{TP}(x_A|x_B)$.

B. Forward Fokker-Planck approach

It is instructive to describe transition paths also using the forward FP equation [4] as this allows to define passage and residence times and to derive various useful relations between transition path times, first-passage times, and passage times.

Defining moments of the Green's function as

$$\mathcal{G}^{(n)}(x|x_0) = \int_0^\infty dt t^n \mathcal{G}(x, t|x_0), \quad (34)$$

we obtain from the forward FP Eq. (4) for $n > 0$ the recursive relations

$$-n \mathcal{G}^{(n-1)}(x|x_0) = \mathcal{L}(x) \mathcal{G}^{(n)}(x|x_0). \quad (35)$$

For $n = 0$ we obtain

$$-\delta(x - x_0) = \mathcal{L}(x) \mathcal{G}^{(0)}(x|x_0). \quad (36)$$

We again impose absorbing boundary conditions at x_A and x_B , i.e. $\mathcal{G}(x_A, t|x_0) = \mathcal{G}(x_B, t|x_0) = 0$, which means that all moments satisfy $\mathcal{G}^{(n)}(x_A|x_0) = \mathcal{G}^{(n)}(x_B|x_0) = 0$. Equations (35) and (36) are solved straightforwardly by integration, yielding

$$\mathcal{G}^{(0)}(x|x_0) = C e^{-F(x)} \{ \phi_A(x_0) \phi_B(x) - \theta(x - x_0) [\phi_A(x_0) - \phi_A(x)] \}, \quad (37)$$

and

$$\mathcal{G}^{(1)}(x|x_0) = C e^{-F(x)} \left\{ \phi_A(x) \int_{x_A}^x dx' \mathcal{G}^{(0)}(x'|x_0) \phi_B(x') + \phi_B(x) \int_x^{x_B} dx' \mathcal{G}^{(0)}(x'|x_0) \phi_A(x') \right\}, \quad (38)$$

where $\theta(x - x_0)$ denotes the Heavyside function with the

properties $\theta(x - x_0) = 1$ for $x > x_0$ and zero otherwise.

Note that we assume the start and end positions x_0 and x of the paths to be inside the absorbing boundary conditions, i.e., $x_A < x < x_B$ and $x_A < x_0 < x_B$. The mean time to reach the position x when starting out from position x_0 follows from proper normalization as

$$\tau^P(x|x_0) = \frac{\mathcal{G}^{(1)}(x|x_0)}{\mathcal{G}^{(0)}(x|x_0)}, \quad (39)$$

we call this time the mean passage time and it is always larger than the mean first-passage time unless the target position is an absorbing boundary. The mean passage time is the mean time to reach the target at position x , while allowing for multiple recrossing events. We obtain for $x_0 < x$ the result

$$\begin{aligned} \tau^P(x|x_0) &= C \frac{\phi_A(x_0)}{\phi_B(x_0)} \int_{x_A}^{x_0} dx' e^{-F(x')} \phi_B^2(x') \\ &+ C \int_{x_0}^x dx' e^{-F(x')} \phi_A(x') \phi_B(x') \\ &+ C \frac{\phi_B(x)}{\phi_A(x)} \int_x^{x_B} dx' e^{-F(x')} \phi_A^2(x'), \end{aligned} \quad (40)$$

while for $x < x_0$ we obtain

$$\begin{aligned} \tau^P(x|x_0) &= C \frac{\phi_A(x)}{\phi_B(x)} \int_{x_A}^x dx' e^{-F(x')} \phi_B^2(x') \\ &+ C \int_x^{x_0} dx' e^{-F(x')} \phi_A(x') \phi_B(x') \\ &+ C \frac{\phi_B(x_0)}{\phi_A(x_0)} \int_{x_0}^{x_B} dx' e^{-F(x')} \phi_A^2(x'). \end{aligned} \quad (41)$$

Obviously, the two expressions are connected by the symmetry $\tau^P(x|x_0) = \tau^P(x_0|x)$ that reflects the reversibility of the underlying processes described by the FP equation. We note that this symmetry also holds when x_0 and/or x are located on the absorbing boundaries x_A and x_B . This symmetry also holds when we shift the absorbing boundary conditions to infinity, i.e. for $x_A \rightarrow -\infty$ and/or $x_B \rightarrow \infty$, that is in the absence of absorbing boundary conditions.

The mean first-passage times in Eqs. (28) and (29) follow from the passage times by the limiting procedures

$$\tau^{FP}(x_A|x_0) = \tau^P(x \rightarrow x_A|x_0), \quad (42)$$

and

$$\tau^{FP}(x_B|x_0) = \tau^P(x \rightarrow x_B|x_0). \quad (43)$$

The expression

$$\begin{aligned} \tau^P(x_0|x_0) &= C \frac{\phi_A(x_0)}{\phi_B(x_0)} \int_{x_A}^{x_0} dx' e^{-F(x')} \phi_B^2(x') \\ &+ C \frac{\phi_B(x_0)}{\phi_A(x_0)} \int_{x_0}^{x_B} dx' e^{-F(x')} \phi_A^2(x'), \end{aligned} \quad (44)$$

measures the mean time a path stays at the starting position x_0 , we call this time the residence time. By explicit consideration of the results in Eqs. (28), (29), (33), (44) it turns out that the transition path time $\tau^{TP}(x_B|x_A)$ in Eq. (33) is related to the first-passage times of reaching the absorbing boundaries at x_A and x_B from an intermediate position x_0 by subtracting the residence time,

$$\tau^{TP}(x_B|x_A) = \tau^{FP}(x_A|x_0) + \tau^{FP}(x_B|x_0) - \tau^P(x_0|x_0). \quad (45)$$

This shows that a transition path time can be constructed by adding the mean first-passage times of two paths starting at an arbitrary position x_0 that reach the boundaries x_A and x_B . Since each path recrosses the starting position, the residence time $\tau^P(x_0|x_0)$ has to be subtracted in order not to overcount these recrossing events. By a tedious but straightforward calculation one can show that

$$\tau^{FP}(x_B|x_0) - \tau^P(x_0|x_0) = \tau^{TP}(x_B|x_0) = \tau^{TP}(x_0|x_B), \quad (46)$$

holds for the transition path time of going from x_0 to x_B or from x_B to x_0 . Combining this with Eq. (45) we thus find

$$\begin{aligned} \tau^{TP}(x_A|x_B) &= \tau^{TP}(x_A|x_0) + \tau^{TP}(x_B|x_0) + \tau^P(x_0|x_0) \\ &= \tau^{FP}(x_A|x_0) + \tau^{TP}(x_0|x_B). \end{aligned} \quad (47)$$

Equation (47) demonstrates that the transition path time from x_A to x_B can be decomposed into the first-passage time starting from an intermediate position x_0 and the transition path time continuing to the other boundary. Together with our definition for the shape of a transition path in Eq. (30), we conclude

$$\begin{aligned} \tau_{shape}^{TP}(x_0|x_A) &= \tau^{TP}(x_B|x_A) - \tau^{TP}(x_B|x_0) \\ &= \tau^{TP}(x_0|x_A) + \tau^P(x_0|x_0), \end{aligned} \quad (48)$$

i.e., the mean shape of a transition path from x_A to x_0 is the transition path time from x_A to x_B minus the transition path time from x_0 to x_B , or, alternatively, the transition path from x_A to x_0 plus the residence time at x_0 .

Finally, and as mentioned before, the symmetry of mean passage times $\tau^P(x|x_0) = \tau^P(x_0|x)$ also holds when we move the point x onto the absorbing boundary x_A , this turns the mean passage time $\tau^P(x_A|x_0)$ into the mean first-passage time and we obtain $\tau^{FP}(x_A|x_0) = \tau^P(x_0|x_A)$. Combining this with the definition Eq. (30) we find

$$\tau_{shape}^{TP}(x_0|x_A) = \tau^{FP}(x_A|x_0) = \tau^P(x_0|x_A), \quad (49)$$

and we see that the transition path shape corresponds to the mean passage time of paths that start from the absorbing boundary x_A . Note that the formulas Eqs. (45)-(49) have been explicitly derived in the presence of absorbing boundaries at positions x_A and x_B , we will show in the next section that similar relation can be derived from integral equations for the distribution of passage times.

C. Renewal equation approach

1. First-passage time distribution

Explicit expressions for the transition path time can also be derived within the renewal equation approach without referral to an explicit underlying diffusive model. The relations derived in this section are thus more general than the previous derivations which were based on the one-dimensional FP equation. Also, the present derivation allows to understand more deeply in what sense the first-passage time $\tau^{FP}(x_A|x_0)$ in the presence of an absorbing boundary at x_B can be interpreted as the shape of a transition path starting from x_A , $\tau_{shape}^{TP}(x_0|x_A)$. In this section we do not impose absorbing boundaries unless explicitly mentioned. Although we use a one-dimensional reaction coordinate, our results can be readily generalized to higher dimensions.

We start with the renewal equation [24, 25]

$$\mathcal{G}(x, t|x_0) = \mathcal{G}_{x'}(x, t|x_0) + \int_0^t dt' \mathcal{G}(x, t-t'|x')K(x', t'|x_0), \quad (50)$$

which can be viewed as a general definition of the first-passage time distribution $K(x', t|x_0)$ and where $\mathcal{G}_{x'}(x, t|x_0)$ denotes the Green's function in the presence of an absorbing boundary condition at x' . It is an alternative more general definition than the one presented in Eq. (12). The renewal equation states that the ensemble of all paths starting at time zero at x_0 and that are at position x at time t can be decomposed into paths that never reach the absorbing boundary condition at x' and paths that hit the boundary x' for the first time at time t' and from there on diffuse freely to x . By letting the position of the absorbing boundary x' coincide with x we obtain the special case

$$\mathcal{G}(x, t|x_0) = \int_0^t dt' \mathcal{G}(x, t-t'|x)K(x, t'|x_0). \quad (51)$$

In terms of the Laplace transform $\tilde{\mathcal{G}}(x, \omega|x_0) = \int_0^\infty dt \mathcal{G}(x, t|x_0)e^{-\omega t}$ Eq. (51) becomes

$$\tilde{\mathcal{G}}(x, \omega|x_0) = \tilde{\mathcal{G}}(x, \omega|x)\tilde{K}(x, \omega|x_0). \quad (52)$$

Using that moments can be calculated from the Laplace transform by

$$\mathcal{G}^{(n)}(x|x_0) \equiv \int_0^\infty dt t^n \mathcal{G}(x, t|x_0) = (-\partial_\omega)^n \tilde{\mathcal{G}}(x, \omega|x_0)|_{\omega=0}, \quad (53)$$

the normalized first moments are related by

$$\begin{aligned} -\partial_\omega \ln \tilde{K}(x, \omega|x_0)|_{\omega=0} &= \frac{K^{(1)}(x|x_0)}{K^{(0)}(x|x_0)} \\ &= \frac{\mathcal{G}^{(1)}(x|x_0)}{\mathcal{G}^{(0)}(x|x_0)} - \frac{\mathcal{G}^{(1)}(x|x)}{\mathcal{G}^{(0)}(x|x)}, \end{aligned} \quad (54)$$

or

$$\tau^{FP}(x|x_0) = \tau^P(x|x_0) - \tau^P(x|x). \quad (55)$$

In other words, the mean first-passage time $\tau^{FP}(x|x_0)$ of going from x_0 to x in the absence of any additional absorbing or reflecting boundaries can be constructed from the mean passage time $\tau^P(x|x_0)$ of going from x_0 to x by subtracting the residence time $\tau^P(x|x)$ of staying at x . By symmetry of the passage time (derived in the previous section) we can write

$$\tau^{FP}(x|x_0) = \tau^P(x_0|x) - \tau^P(x|x). \quad (56)$$

This relation holds also in the presence of an absorbing boundary condition at x_0 (note that an absorbing boundary condition can be simply imposed by creating a potential well of infinite depth in the region $x < x_0$, which turns x_0 into an absorbing boundary for all paths that come from $x > x_0$). This turns $\tau^{FP}(x|x_0)$ into the transition path time $\tau^{TP}(x|x_0)$, the passage time $\tau^P(x_0|x)$ into the first-passage time $\tau^{FP}(x_0|x)$, and the residence time $\tau^P(x|x)$ without specified boundary conditions into the residence time at x in the presence of an absorbing boundary at x_0 , which we denote by $\tau_{x_0}^P(x|x)$. We thus obtain from Eq. (56)

$$\tau^{TP}(x|x_0) = \tau^{TP}(x_0|x) = \tau^{FP}(x_0|x) - \tau_{x_0}^P(x|x), \quad (57)$$

which is equivalent to Eq. (46) (note that Eq. (46) by way of derivation holds in the presence of two absorbing boundary conditions at x_A and x_B , so to make the equivalence perfect we can either shift the boundary x_A in Eq. (46) to infinity or impose an additional absorbing boundary condition in Eq. (57)).

In order to derive Eq. (47) we need a convolution equation for first-passage times. For this we choose in the renewal equation (50) the absorbing boundary condition x' at a relative position $x_0 < x' < x$ and in this case obtain

$$\mathcal{G}(x, t|x_0) = \int_0^t dt' \mathcal{G}(x, t-t'|x')K(x', t'|x_0). \quad (58)$$

We now impose an absorbing boundary condition at x , which turns both Green's functions into first-passage time distributions so that we obtain

$$K(x, t|x_0) = \int_0^t dt' K(x, t-t'|x')K(x', t'|x_0), \quad (59)$$

valid for arbitrary positions x' with $x_0 < x' < x$. By using Laplace transformation, similarly as the calculation leading to Eq. (55), this yields

$$\tau^{FP}(x|x_0) = \tau^{FP}(x'|x_0) + \tau^{FP}(x|x'). \quad (60)$$

Imposing an additional absorbing boundary condition at x_0 turns this into

$$\tau^{TP}(x|x_0) = \tau^{TP}(x'|x_0) + \tau_{x_0}^{FP}(x|x'), \quad (61)$$

where the subindex x_0 in the last term indicates that an absorbing boundary is present at x_0 . This is identical to Eq. (47), remembering that Eq. (47) was derived in the presence of an absorbing boundary at x_B . We next combine Eqs. (57) and (61) and obtain

$$\tau^{TP}(x|x_0) = \tau_{x_0}^{FP}(x|x') + \tau^{FP}(x_0|x') - \tau_{x_0}^P(x'|x'), \quad (62)$$

which is equivalent Eq. (45) if we impose an additional absorbing boundary condition at x .

2. Transition path time distribution

We now impose an absorbing boundary condition at position x_0 in the convolution equation (59), this turns the two first-passage time distributions starting at x_0 into transition path time distributions and we obtain

$$T(x, t|x_0) = \int_0^t dt' K_{x_0}(x, t-t'|x')T(x', t'|x_0), \quad (63)$$

where $K_{x_0}(x, t-t'|x')$ is the first-passage time distribution with an additional absorbing boundary condition at x_0 with $x_0 < x' < x$. Note that Eq. (61) follows directly from this integral equation via Laplace transformation. It means that a transition path can be decomposed into a transition path to an intermediate position x' followed by a first-passage path from x' that does not revisit x_0 .

To go on with our derivation we define the last-passage distribution via the integral equation

$$\mathcal{G}(x, t|x_0) = \mathcal{G}_{x'}(x, t|x_0) + \int_0^t dt' H(x, t-t'|x')\mathcal{G}(x', t'|x_0). \quad (64)$$

In essence, the last-passage distribution $H(x, t'|x')$ comprises all paths that go from x' to x without revisiting the starting point at x' . By moving the starting position x_0 to the absorbing boundary at x' we obtain

$$\mathcal{G}(x, t|x') = \int_0^t dt' H(x, t-t'|x')\mathcal{G}(x', t'|x'). \quad (65)$$

We now impose two absorbing boundary conditions, one at x and the other at x_0 with the condition $x_0 < x' < x$, and obtain

$$K_{x_0}(x, t|x') = \int_0^t dt' T(x, t-t'|x')\mathcal{G}_{x_0, x}(x', t'|x'). \quad (66)$$

By inserting this integral equation into Eq. (63) we obtain

$$T(x, t|x_0) = \int_0^t dt' \int_0^{t-t'} dt'' T(x, t-t'-t''|x')\mathcal{G}_{x_0, x}(x', t''|x')T(x', t'|x_0), \quad (67)$$

which has a nice intuitive interpretation: a transition path from x_0 to x can be decomposed into a transition path from x_0 to an arbitrary mid-point position x' , a path that starts from x' and returns to x' without reaching the

boundaries at x_0 and x , and finally a transition path from x' to the final destination x .

We now use the renewal equation (51) and impose an absorbing boundary condition at x_0 and replace the variable x by x' to yield

$$H(x', t|x_0) = \int_0^t dt' \mathcal{G}_{x_0}(x', t-t'|x')T(x', t'|x_0), \quad (68)$$

which is an explicit integral equation for the last-passage time distribution. We now impose an additional absorbing boundary condition at x with the ordering $x_0 < x' < x$ and obtain

$$H_x(x', t|x_0) = \int_0^t dt' \mathcal{G}_{x_0, x}(x', t-t'|x')T(x', t'|x_0). \quad (69)$$

By comparison with Eq. (67) we obtain

$$T(x, t|x_0) = \int_0^t dt' T(x, t-t'|x')H_x(x', t'|x_0). \quad (70)$$

Also this expression, from which we will derive the transition path shape, has an intuitive interpretation: a transition path from x_0 to x can be decomposed into a last-passage path from x_0 to an arbitrary mid-point position x' followed by a transition path from x' to the final destination x . Note that the last-passage paths from x_0 to x' do not visit the absorbing boundary condition x which is indicated by the subscript.

By construction, the integrand in Eq. (70) is the joint probability that a transition path starting from x_0 and ending at x has a duration of t and is at time t' at the position x' . This is so because paths for times later than t' proceed on transition paths to x and do not visit back to x' and therefore do not contribute to the probability of being at x' . The average shape of a transition path thus is obtained by averaging the $T(x, t-t'|x')H_x(x', t'|x_0)$ both over the intermediate time t' and transition path duration t . We thus obtain for the shape of a transition path from x_A to x_B

$$\tau_{shape}^{TP}(x|x_A) = \frac{\int_0^\infty dt \int_0^t dt' t' T(x_B, t-t'|x)H_{x_B}(x, t'|x_A)}{\int_0^\infty dt \int_0^t dt' T(x_B, t-t'|x)H_{x_B}(x, t'|x_A)}. \quad (71)$$

By slightly rearranging we obtain

$$\tau_{shape}^{TP}(x|x_A) = \frac{\int_0^\infty dt' t' H_{x_B}(x, t'|x_A)}{\int_0^\infty dt' H_{x_B}(x, t'|x_A)} = \tau_{x_A, x_B}^P(x|x_A), \quad (72)$$

and thus have derived the important result that the shape of a transition path is given by the passage time from an absorbing boundary at x_A to a midpoint x in the presence of a second absorbing boundary at x_B , as presented in Eq. (49). We remind the reader of the relation Eq. (49) which shows that because of the symmetry of passage times, instead of averaging over paths that come from the absorbing boundary x_A , one can equally well average over first-passage paths that start from x and

that end at the boundary x_A , the latter ensemble is for simulations much more easy to implement and we will explicitly demonstrate the equivalence of both ensembles in our simulations.

III. THE SHAPE OF KRAMERS' FIRST-PASSAGE PATHS

Here we consider the mean shape of the Kramers' first-passage paths defined as paths that start from a reflecting boundary and reach an absorbing boundary. We basically repeat the derivation steps from the previous section but replace the absorbing boundary condition at x_A by a reflecting one. If we impose a reflecting boundary at position x_A in the convolution relation for the first-passage distribution Eq. (59) we obtain

$$K_{\tilde{x}_A}(x_B, t|x_A) = \int_0^t dt' K_{\tilde{x}_A}(x_B, t-t'|x) K_{\tilde{x}_A}(x, t'|x_A), \quad (73)$$

where we denote a reflecting boundary condition by a subscript with a tilde and an adsorbing boundary condition by a subscript without a tilde.

We next impose an absorbing boundary condition at x_B and a reflecting boundary condition at x_A in the integral relation for the last-passage distribution Eq. (65) and obtain

$$K_{\tilde{x}_A}(x_B, t|x') = \int_0^t dt' T(x_B, t-t'|x) \mathcal{G}_{\tilde{x}_A, x_B}(x, t'|x). \quad (74)$$

By inserting this integral equation into Eq. (73) we obtain

$$K_{\tilde{x}_A}(x_B, t|x_A) = \int_0^t dt' \int_0^{t-t'} dt'' T(x_B, t-t'-t''|x) \mathcal{G}_{\tilde{x}_A, x_B}(x, t''|x) K_{\tilde{x}_A}(x, t'|x_A), \quad (75)$$

which has a similar interpretation as the corresponding result for an absorbing boundary condition at the origin in Eq. (67): a Kramers' first-passage path from x_A to x_B can be decomposed into a first-passage path from x_A to an arbitrary mid-point position x , a path that starts from x and returns to x without reaching the absorbing boundary at x_B and without crossing the reflecting boundary at x_A , and finally a transition path from x to the final destination x_B .

We next impose an absorbing boundary condition at x_B and a reflecting boundary condition at $x_0 = x_A$ on the definition of the first-passage distribution Eq. (51), from which we obtain

$$\mathcal{G}_{\tilde{x}_A, x_B}(x, t|x_A) = \int_0^t dt' \mathcal{G}_{\tilde{x}_A, x_B}(x, t-t'|x) K_{\tilde{x}_A}(x, t'|x_A). \quad (76)$$

Comparison with Eq. (75) gives the integral equation

$$K_{\tilde{x}_A}(x_B, t|x_A) = \int_0^t dt' T(x_B, t-t'|x) \mathcal{G}_{\tilde{x}_A, x_B}(x, t|x_A). \quad (77)$$

We now use similar arguments leading to our expression for the transition path shape in Eq. (72): The integrand in Eq. (77) is the joint probability that a first-passage path starting from x_A and ending at x_B has a duration of t and is at time t' at position x . The average shape of a first-passage path is obtained by averaging over both intermediate time t' and the first-passage path duration t , we thus obtain for the mean shape of a Kramers' first-passage path from x_A to x_B

$$\tau_{shape}^{KFP}(x|x_A) = \frac{\int_0^\infty dt' t' \mathcal{G}_{\tilde{x}_A, x_B}(x, t'|x_A)}{\int_0^\infty dt' \mathcal{G}_{\tilde{x}_A, x_B}(x, t'|x_A)} = \tau_{\tilde{x}_A, x_B}^P(x|x_A). \quad (78)$$

The only difference to the result for the transition path shape Eq. (72) is that the absorbing boundary condition at x_A is replaced by a reflecting boundary condition.

By Laplace transformation of Eq. (77) we obtain (similarly as when we derived Eq. (55) from Eq. (51))

$$\tau^{KFP}(x_B|x_A) = \tau^{TP}(x_B|x) + \tau_{\tilde{x}_A, x_B}^P(x|x_A), \quad (79)$$

where we defined the Kramers' mean first-passage time as $\tau^{KFP}(x_B|x_A) = \tau_{shape}^{KFP}(x_B|x_A)$ and which is explicitly given by [26]

$$\tau^{KFP}(x_B|x_A) = \int_{x_A}^{x_B} dx \frac{e^{F(x)}}{D(x)} \int_{x_A}^x dx' e^{-F(x')}. \quad (80)$$

By combining Eq. (48), Eq. (78) and Eq. (79) we find

$$\tau_{shape}^{KFP}(x|x_A) = \tau_{shape}^{TP}(x|x_A) + \tau_{\tilde{x}_A, x_B}^P(x_A|x_A), \quad (81)$$

showing that the mean shape of Kramers' first-passage paths $\tau_{shape}^{KFP}(x|x_A)$ and the mean shape of transition paths $\tau_{shape}^{TP}(x|x_A)$ are identical and shifted by a constant given by $\tau_{\tilde{x}_A, x_B}^P(x_A|x_A)$. This shift corresponds to the passage time at the reflecting boundary x_A and is according to Eq. (79) given by $\tau_{\tilde{x}_A, x_B}^P(x_A|x_A) = \tau^{KFP}(x_B|x_A) - \tau^{TP}(x_B|x)$.

IV. RESULTS FOR EXPLICIT POTENTIALS

We next present exemplaric transition path shapes for a few different simple potential shapes shown in Fig. 1-(a)-(c). We consider a reaction coordinate x in the range of $0 \leq x \leq L$, where L is the transition length scale, and restrict ourselves from now on to a homogeneous diffusion constant D

A. Brownian dynamics simulations and trajectory analysis

We also present trajectories obtained from one dimensional overdamped Brownian dynamics (BD) simulations. The simulations are based on the Langevin equation

$$\frac{dx(t)}{dt} = -D \frac{dF(x)}{dx} + \frac{\zeta(t)}{\gamma}, \quad (82)$$

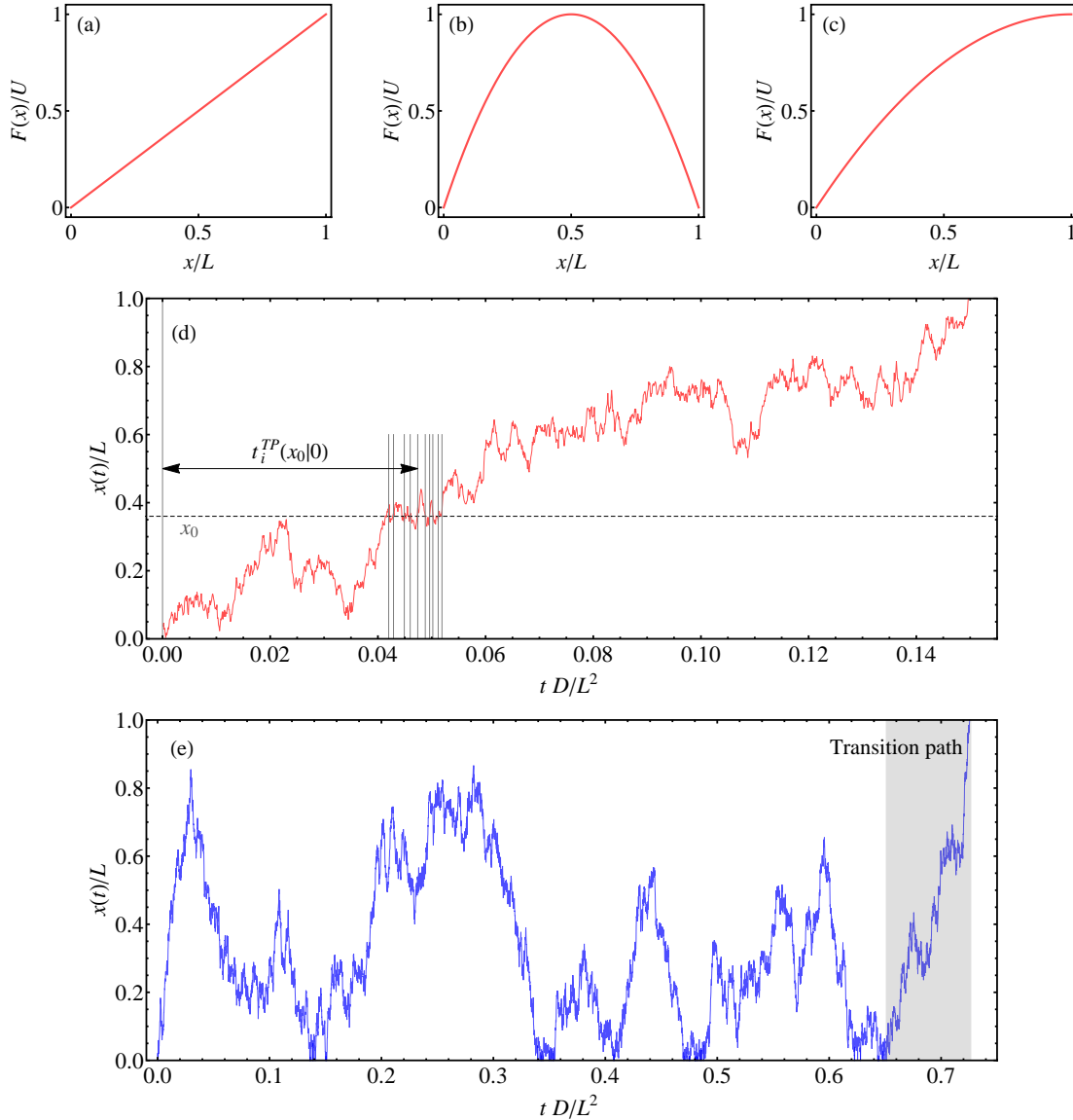


FIG. 1: Illustrations of the used rescaled potentials $F(x)/U$ as a function of the rescaled length x/L , where L is the transition length scale and U is the barrier height: (a) linear potential $F(x) = Ux/L$, (b) full harmonic potential $F(x) = 4U(1-x/L)x/L$ and (c) harmonic ramp $F(x) = U(2-x/L)x/L$. (d) A typical transition path trajectory $x^{TP}(t)$ for the force-free case, obtained from Brownian dynamics (BD) simulations. The times $t_i^{TP}(x_0|0)$ when the transition path crosses the position x_0 are indicated by vertical lines. (e) A typical Kramers' first-passage path trajectory $x^{KFP}(t)$ for the force-free case, obtained from BD simulations, in the presence of a reflecting boundary condition at $x = 0$ and an absorbing boundary condition at $x = L$. The transition path is the last part of the trajectory indicated by the gray region.

where $\gamma = k_B T/D$ is the friction constant and $\zeta(t)$ is a Gaussian random force which fulfills $\langle \zeta(t) \rangle = 0$ and $\langle \zeta(t)\zeta(t') \rangle = 2\gamma k_B T \delta(t-t')$. The discretized and rescaled Langevin equation reads

$$\tilde{x}(\tilde{t} + d\tilde{t}) = \tilde{x}(\tilde{t}) - \frac{dF}{d\tilde{x}} d\tilde{t} + \sqrt{2d\tilde{t}} r(\tilde{t}), \quad (83)$$

where $\tilde{x} = x/L$ is the rescaled position, $\tilde{t} = tD/L^2$ is the rescaled time, and $r(\tilde{t})$ is a Gaussian random number

with zero mean and unit standard deviation. We iterate Eq. (83) with a typical time step $d\tilde{t} = 10^{-4}$.

To obtain mean first-passage times $\tau^{FP}(0|x_0)$ and $\tau^{FP}(L|x_0)$ we vary the initial position from $x_0 = 0$ to $x_0 = L$ and measure the time needed to reach one of the two absorbing boundaries $x_A = 0$ or $x_B = L$ for the first time, we typically average over 10^5 first-passage times.

We also generate transition path trajectories within BD simulations. In practice we initiate a trajectory at a

reflecting boundary at $x = 0$ and record until it reaches the absorbing boundary at $x = L$, the transition path trajectory is the last portion of the trajectory after it has last returned to the reflecting boundary at $x = 0$, as shown in Fig. 1-(e). The mean transition path shape is obtained by averaging the time transition paths take to reach a certain position x_0

$$\tau_{shape}^{TP}(x_0|0) = \sum_{i=1}^N \frac{t_i^{TP}(x_0|0)}{N}, \quad (84)$$

where $t_i^{TP}(x_0|0)$ denotes the time at which a transition path trajectory that starts out at $x = 0$ crosses the position x_0 , as illustrated in Fig. 1-(d). Note that a single transition path crosses the position x_0 multiple times, the averaging in Eq. (84) is done over the entire transition path ensemble and over all crossing events, N thus counts the total number of crossing events in the entire transition path ensemble. For our final results we typically generate 10^4 transition paths.

In a similar manner, we analyze Kramers' first-passage trajectories, which start from a reflecting boundary at $x = 0$ and eventually reach the absorbing boundary at $x = L$, an example of which is shown in Fig. 1-(e). To obtain the mean shape of Kramers' first-passage trajectories, denoted by $\tau_{shape}^{KFP}(x_0|0)$, we average the mean time it takes such a path to reach a certain position x_0

$$\tau_{shape}^{KFP}(x_0|0) = \sum_{i=1}^N \frac{t_i^{KFP}(x_0|0)}{N}, \quad (85)$$

where $t_i^{KFP}(x_0|0)$ denotes the time at which a path that starts from $x = 0$ crosses $x = x_0$.

B. Force-free case

We first consider the force-free case, $F = 0$. The splitting probabilities read $\phi_A(x) = 1 - x/L$ and $\phi_B(x) = x/L$ with $C = 1$, and the transition path time according to Eq. (33) reads

$$\tau^{TP}(L|0) = \frac{L^2}{6D}, \quad (86)$$

which is three times smaller than Kramers' mean first-passage time

$$\tau^{KFP}(L|0) = \frac{L^2}{2D}, \quad (87)$$

according to Eq. (80). This decrease is due to the subtraction of the part of the Kramers' first-passage trajectories that contains multiple returns to the origin, as illustrated in Fig. 1-(e).

The normalized distribution functions for the transition path time $\tau^{TP}(L|0)$ (circles) and the Kramers' first-passage time $\tau^{KFP}(L|0)$ (squares) are shown in Fig. 2-(a), obtained from BD simulations. The transition path

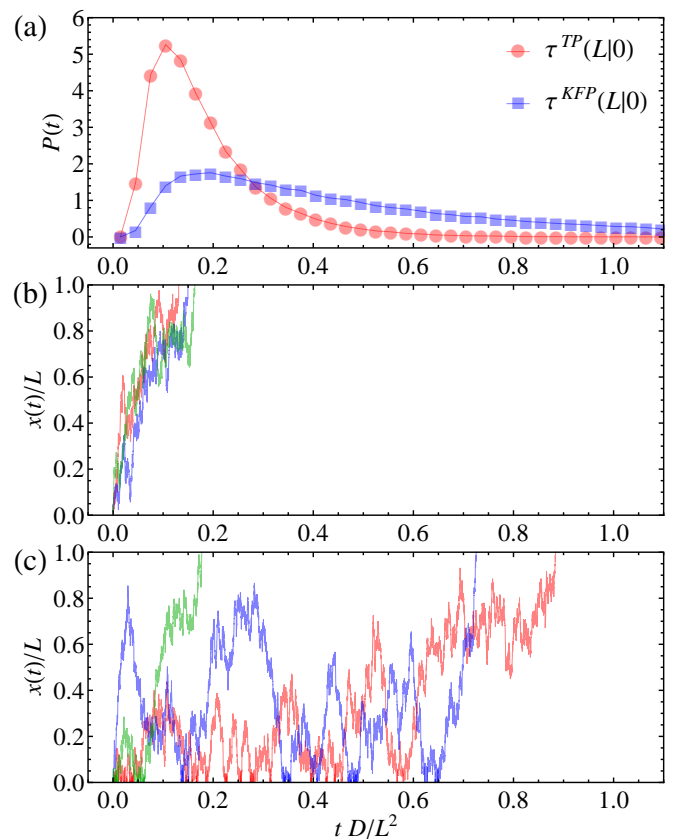


FIG. 2: (a) The normalized distribution functions for the transition path time $\tau^{TP}(L|0)$ (circles) and the Kramers' first-passage time $\tau^{KFP}(L|0)$ (squares) in the force-free case, obtained from BD simulations. (b) Three typical transition path trajectories $x(t)$. (c) Three typical Kramers' first-passage trajectories $x(t)$.

time distribution is more sharply peaked compared with the Kramers' first-passage time distribution. The trajectories shown in Fig. 2-(b) and (c) reflect this difference of the two distributions.

The mean transition path shape is, according to Eqs. (28) and (30), given as

$$\tau_{shape}^{TP}(x_0|0) = \tau^{FP}(0|x_0) = \frac{Lx_0}{6D} \left(2 - \frac{x_0}{L} \right), \quad (88)$$

and is depicted in Fig. 3-(a) by a solid line. Note that the transition path shape is a quadratic function, transition paths start out with finite velocity at the origin and reach the final destination with infinite velocity. This asymmetry, which is a universal property of mean transition path shapes for all potentials, can be easily understood by considering Eq. (48) and realizing that a mean transition path time scales quadratically with the diffusion length scale in the limit of small diffusion length scale. The filled symbols in Fig. 3-(a) show the BD simulation results for the first-passage time $\tau^{FP}(0|x_0)$ while the open square symbols show the BD results for $\tau_{shape}^{TP}(x_0|0)$ obtained via Eq. (84), both simulation results agree well with the

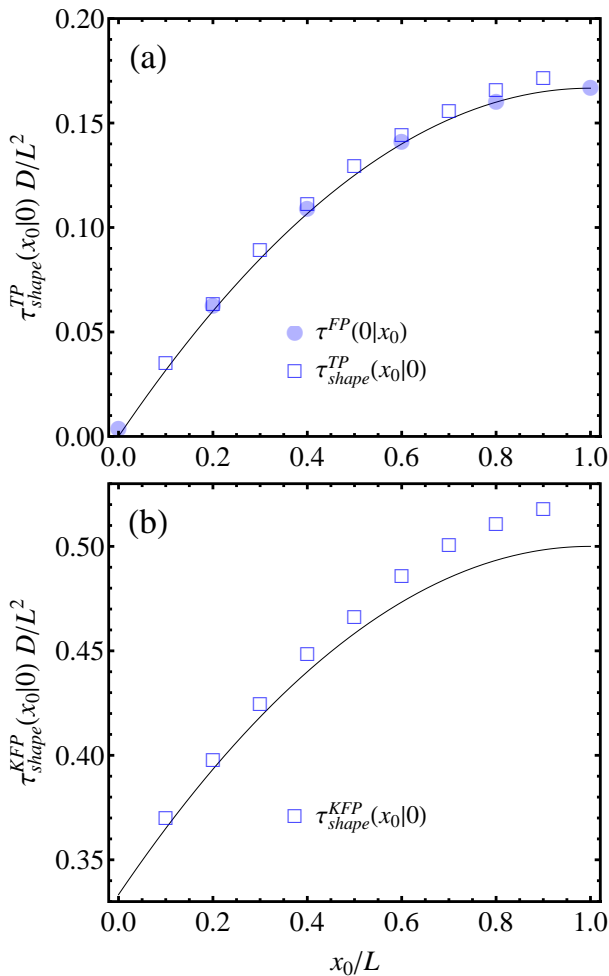


FIG. 3: (a) Mean shape of transition paths $\tau_{shape}^{TP}(x_0|0)$ in the force-free case. The solid line shows the analytic result Eq. (88). Filled circles show BD simulation results for the mean first-passage time $\tau^{FP}(0|x_0)$ while open squares show the mean shape from the analysis of transition paths according to Eq. (84). (b) Mean shape of Kramers' first-passage paths $\tau_{shape}^{KFP}(x_0|0)$ in the force-free case. Symbols show BD simulation results while the solid line shows analytic results according to Eqs. (81) and (88). Note that the two curves in (a) and (b) are identical except a vertical shift by a constant time.

theoretical result Eq. (88).

The transition path shapes read

$$\tau_{shape}^{TP}(x_0|0) = \frac{L^2}{D} \frac{\operatorname{csch}\left(\frac{U}{2}\right) \operatorname{csch}\left(\frac{U}{2} - \frac{Ux_0}{2L}\right) \left[(x_0/L - 2) \sinh\left(\frac{Ux_0}{2L}\right) + \frac{x_0}{L} \sinh\left(U - \frac{Ux_0}{2L}\right) \right]}{2U}, \quad (91)$$

$$\tau_{shape}^{TP}(x_0|L) = \frac{L^2}{D} \frac{\coth(U/2) - \frac{x_0}{L} \coth(Ux_0/2L)}{U}, \quad (92)$$

The solid curve in Fig. 3-(b) shows the Kramers' mean first-passage shape $\tau_{shape}^{KFP}(x_0|0)$, calculated from Eqs. (81) and (88). The Kramers' mean first-passage shape $\tau_{shape}^{KFP}(x_0|0)$ is, according to Eqs. (79) and (81), identical to the transition path shape $\tau^{TP}(x_0|0)$ shifted by the amount $\tau_{\tilde{x}_A=0, \tilde{x}_B=L}^P(x) = \tau^{KFP}(L|0) - \tau^{TP}(L|0) = L^2/(3D)$. The symbols in Fig. 3-(b) show the BD results using Eq. (85), again, the agreement is very good.

C. Transition path in linear potential

For a linear potential $F = Ux/L$ we find for the transition path time

$$\tau^{TP}(L|0) = \frac{L^2 U \coth\left(\frac{U}{2}\right) - 2}{D U^2}, \quad (89)$$

which is an even function of U . This means that the transition path time is the same irrespective of whether the transition paths go up the linear potential or whether they go down. This of course follows directly from the general symmetry of passage times in Eqs. (40) and (41) but is worthwhile pointing out again at this point. To leading order in U the asymptotic behavior reads

$$\tau^{TP} D/L^2 \approx \begin{cases} \frac{1}{6} - \frac{U^2}{360} & , |U| \ll 1 \\ 1/|U| & , |U| \gg 1. \end{cases} \quad (90)$$

The red solid curve in Fig. 4-(a) shows $\tau^{TP}(L|0)$ in Eq. (89) while the asymptotic expressions in Eq. (90) are depicted by broken curves. Note that the Kramers' mean first-passage time $\tau^{KFP}(L|0) = L^2(e^U - 1 - U)/(DU^2)$, shown by a solid blue curve in Fig. 4-(a), shows very different behavior and in particular is a monotonically increasing function of U . For large potential strength $U \gg 1$ we find an exponential increase to leading order, $\tau^{KFP}(L|0) \sim e^U/U^2$. The symbols in Fig. 4-(a) show BD simulation results for the transition path time, which agree well with the theory.

A further noteworthy fact is that the mean transition path time τ^{TP} is for non-zero values of U strictly smaller than the force-free result $\tau^{TP} = L^2/(6D)$ corresponding to the maximum value obtained for $U = 0$. This means that transition paths in a linear potential are faster than force-free transition paths, regardless of whether the slope is positive or negative.

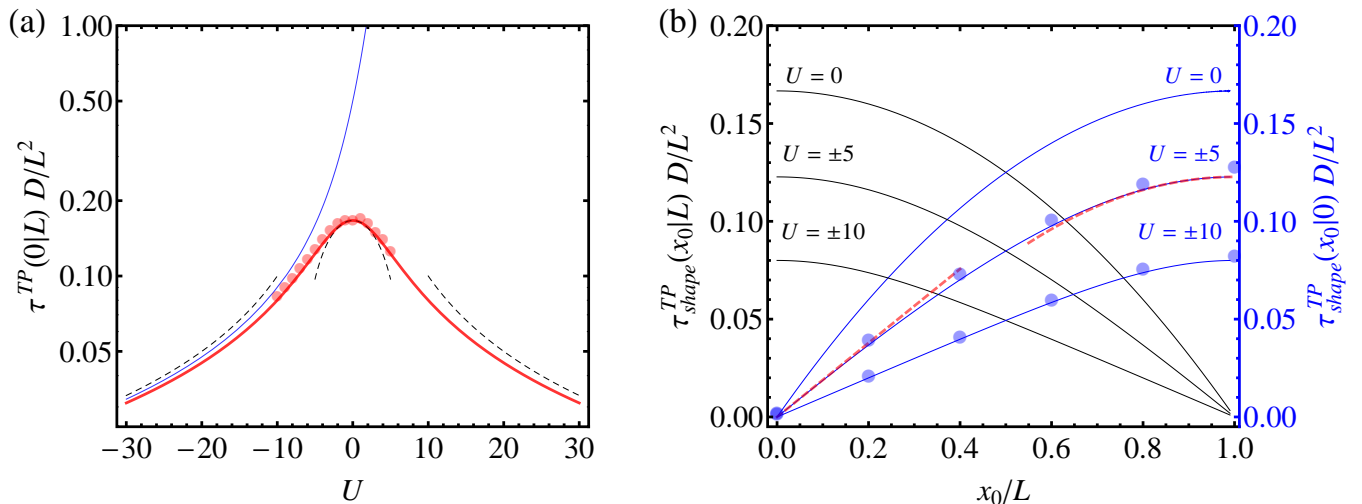


FIG. 4: Results for a linear potential $F = Ux/L$. (a) The solid red curve shows the mean transition path time $\tau^{TP}(0|L)$ from Eq. (89) as a function of U on a log-linear scale. The broken curves depict the asymptotic expressions from Eq. (90). For comparison, the solid blue curve shows Kramers' mean first-passage time $\tau^{KFP}(L|0)$ which monotonically increases with U . The symbols denote BD simulation results. (b) Mean shapes of transition paths τ_{shape}^{TP} . Blue curves depict $\tau_{shape}^{TP}(x_0|0)$ starting from the left boundary from Eq. (91), while black curves depict $\tau_{shape}^{TP}(x_0|L)$ starting from the right boundary from Eq. (92). Symbols denote BD simulation results for $U = -5$ and $U = -10$ while broken red curves depict the asymptotic expressions for $U = \pm 5$ from Eq. (93).

where $\tau_{shape}^{TP}(x_0|0)$ has the asymptotic limits

$$\tau_{shape}^{TP}(x_0|0)D/L^2 \approx \begin{cases} \frac{U - \sinh U}{U(1 - \cosh U)} \frac{x_0}{L} & , x_0 \ll L \\ \tau^{TP}(L|0)D/L^2 - \frac{1}{6} \left(\frac{x_0}{L} - 1\right)^2 & , x_0 \approx L. \end{cases} \quad (93)$$

Figure 4-(b) shows the transition path shapes τ_{shape}^{TP} as function of the position x_0 , where the blue curves depict $\tau_{shape}^{TP}(x_0|0)$ in Eq. (91), and the black curves depict $\tau_{shape}^{TP}(x_0|L)$ in Eq. (92). Symbols denote BD simulation results for $U = -5$ and $U = -10$. The broken red curves depict the asymptotic limits in Eq. (93) for $U = \pm 5$. Due to the symmetry of passage times, the shapes τ_{shape}^{TP} are symmetric with respect to an exchange of starting positions.

D. Harmonic potential

For a harmonic potential $F = 4Ux(1-x/L)/L$ we find for the transition path time

$$\tau^{TP}(L|0) = \frac{L^2}{4D} F_{2,2}(-U) - \frac{L^2}{2D\sqrt{\pi}U \operatorname{erf}(\sqrt{U})} \int_0^{\sqrt{U}} dy y^2 e^{-y^2} F_{2,2}(-y^2), \quad (94)$$

where $F_{2,2}(x) = F_{2,2}(\{1, 1\}; \{3/2, 2\}; x)$ is the generalized hypergeometric function. For the small barrier limit $|U| \ll 1$ we find to leading order

$$\tau^{TP}(L|0) \approx \frac{L^2}{D} \left[\frac{1}{6} - \frac{2}{45}U \right], \quad (95)$$

which decreases from the force-free transition path time $\tau^{TP} = L^2/(6D)$. For the large barrier limit $U \rightarrow \infty$ we recover the known asymptotic result [5, 7]

$$\tau^{TP}(L|0) \approx \frac{L^2 \ln(2e^\gamma U)}{8DU}, \quad (96)$$

where $\gamma \approx 0.577$ is the Euler gamma constant, and we used $\operatorname{erf}(\sqrt{U}) \approx 1$, $F_{2,2}(-U) \approx \ln(4e^\gamma U)/(2U)$ and $\int_0^\infty dy y^2 e^{-y^2} F_{2,2}(-y^2) = (\sqrt{\pi}/4) \ln(2)$ for large U . We note that the denominator $8U$ in Eq. (96) can be reinterpreted as the rescaled curvature $\omega^2 = L^2 |(d^2F/dx^2)_{x=L/2}|$ at the barrier top of the harmonic potential, yielding the previously published form [7]

$$\tau^{TP}(L|0) \approx \frac{L^2 \ln(2e^\gamma U)}{D\omega^2}. \quad (97)$$

For fixed potential curvature and varying potential height, Eq. (97) shows that the transition path time increases logarithmically with increasing potential height U , while for fixed diffusion L , Eq. (96) shows that the transition path time decreases inversely linearly with increasing potential height U [5].

In Fig. 5 we present $\tau^{TP}(L|0)$ as a function of the barrier height U . In Fig. 5-(a) we show $\tau^{TP}(L|0)D/L^2$ from Eq. (94) on a log-log scale (solid red curve), which is seen to decrease from the force-free case $\tau^{TP}D/L^2 = 1/6$ as U increases. We also show the asymptotic expressions Eqs. (95) and (96) by dashed curves. In Fig. 5-(b) we show $\tau^{TP}(L|0)$ from Eq. (94) on a log-linear scale (solid red curve), here we also compare with BD simulation results obtained via Eq. (84). The solid blue curves in Fig. 5 depict the Kramers' mean first-passage time given by

$$\tau^{KFP}(L|0) = \frac{L^2 \pi \operatorname{erf}(\sqrt{U}) \operatorname{erfi}(\sqrt{U})}{D 8U}, \quad (98)$$

where $\operatorname{erf}(x) = \frac{2}{\sqrt{\pi}} \int_0^x e^{-t^2} dt$ is the error function, and $\operatorname{erfi}(x) = \frac{2}{\sqrt{\pi}} \int_0^x e^{t^2} dt$ is the imaginary error function. The leading order result for large $|U|$ reads

$$\tau^{KFP}(L|0)D/L^2 = \frac{\sqrt{\pi}}{8} \frac{e^{|U|}}{|U|^{3/2}} = \frac{\sqrt{\pi}}{\omega^2} \frac{e^{|U|}}{\sqrt{|U|}}. \quad (99)$$

In Fig. 5 we see that the transition path time $\tau^{TP}(L|0)$ is a monotonically decreasing function of the barrier height U , while the Kramers' time $\tau^{KFP}(L|0)$ is a symmetric function and has a minimum of $\tau^{KFP} = L^2/(2D)$

at $U = 0$. In fact, transition paths over a harmonic barrier with $U > 0$ are faster, while transition paths over a harmonic well characterized by $U < 0$ are slower compared to the force-free case with $U = 0$. This can be rationalized by Eq. (47), since the transition path time for reaching from the boundaries to the center of the harmonic potential are rather insensitive on whether U is positive or negative (as will be shown in the next section), but the residence time at the center of the harmonic potential is much larger for the case of a harmonic well with $U < 0$ than for a harmonic barrier with $U > 0$. The symmetric behavior of the Kramers' mean first-passage time can be understood based on Eq. (60) since first-passage time are transitive: the first-passage time for traversing a harmonic potential is the sum of the first-passage times from the boundary to the middle and from the middle to the other boundary. We reiterate that mean first-passage times are transitive, as shown in Eq. (60), while transition path times are not, as shown in Eq. (47).

In Fig. 6 we show the normalized distribution functions for the transition path time (circles) and for the Kramers' first-passage time (squares) for $U = 3$, obtained from BD simulations. The transition path time distribution shows a pronounced peak around $\tau D/L^2 = 0.1$, close to the mean transition path time $\tau^{TP}(L|0)(U = 3)D/L^2 \approx 0.1$, as seen in Fig. 5. In contrast, the Kramers' first-passage time distribution is quite broad, the first moment is given by $\tau^{KFP}(L|0)(U = 3)D/L^2 \approx 1$ and thus is 10 times larger than the mean transition path time.

For the transition path shape we find

$$\tau_{shape}^{TP}(x_0|0) = \tau^{TP}(L|0) - \frac{L^2}{2DU} \int_{\sqrt{U}}^{\sqrt{U}(2x_0/L-1)} dy \left(\frac{\operatorname{erf}(y) - \operatorname{erf}(\sqrt{U})}{\operatorname{erf}(\sqrt{U}(2x_0/L-1)) - \operatorname{erf}(\sqrt{U})} - \frac{1}{2} \right) D_+(y), \quad (100)$$

where $D_+(x) = e^{-x^2} \int_0^x dt e^{t^2}$ is the Dawson integral function. The second term in Eq. (100) vanishes for $x_0 = L$ and reduces to $-\tau^{TP}(L|0)$ given in Eq. (94) for $x_0 = 0$.

Figure 7 depicts the mean transition path shapes $\tau_{shape}^{TP}(x_0|0)$ in Eq. (100) for different values of the barrier height U . Transition paths are faster for positive values of U , i.e. for paths that have to go over a harmonic barrier top, while the slow down for negative values of U , i.e. for paths that have to traverse a harmonic well. Again, we observe a pronounced asymmetry of the mean shape of transition paths, paths start out quickly and reach the boundary at $x = L$ with vanishing slope. Filled symbols show BD simulation results for $\tau^{FP}(0|x_0)$ while open symbols show BD simulation results for $\tau_{shape}^{TP}(x_0|0)$, both for $U = 3$. We observe good agreement between the two different ways of extracting

transition path shapes, as expected based on our analytical results, as well as with our analytically derived shape.

E. Harmonic ramp

Here we consider the harmonic potential $F(x) = Ux(2 - x/L)/L$ which has a barrier top $F = U$ at the final position $x = L$.

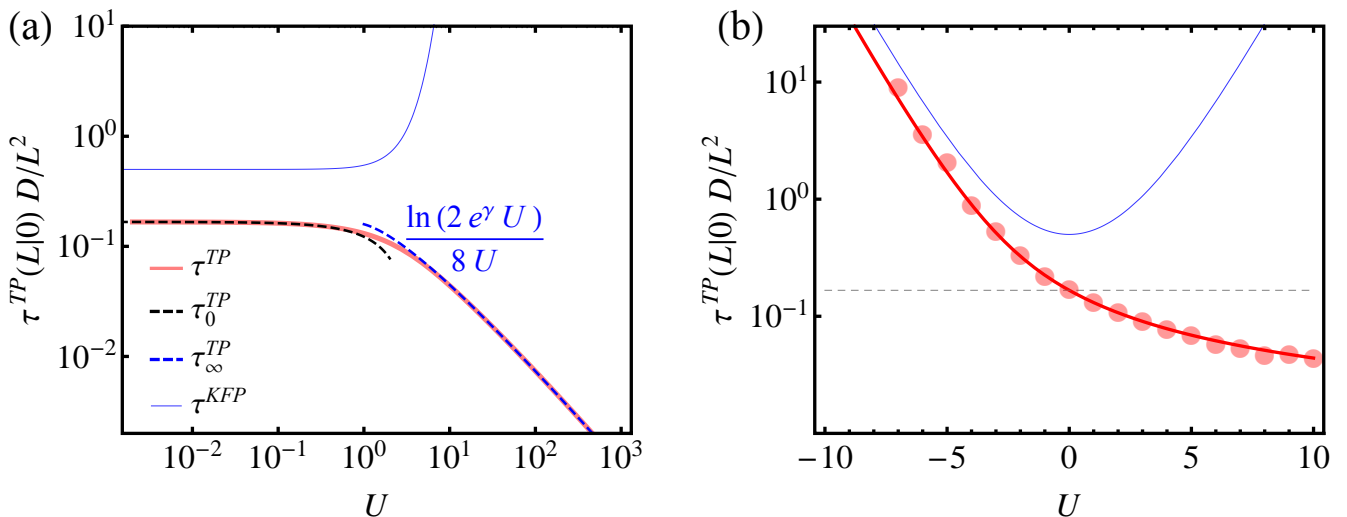


FIG. 5: Results for the harmonic potential $F = 4Ux(1-x/L)/L$ as a function of the barrier height U . (a) Mean transition path time $\tau^{TP}(L|0)$ from Eq. (94) (solid red curve) on a log-log scale, compared with the asymptotic expressions Eqs. (95) and (96) (dashed lines). (b) Mean transition path time $\tau^{TP}(L|0)$ (solid red curve) on a log-linear compared with BD simulation data (symbols). Solid blue curves depict the Kramers' mean first-passage time $\tau^{KFP}(L|0)$ from Eq. (98). The horizontal dashed line depicts the force-free transition path time $\tau^{TP} = L^2/(6D)$.

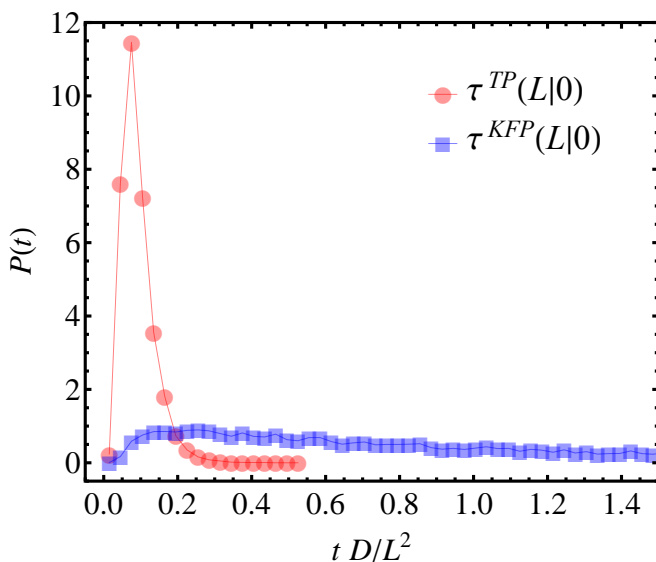


FIG. 6: Normalized distribution functions for the transition path time $\tau^{TP}(L|0)$ (circles) and the Kramers' first-passage time $\tau^{KFP}(L|0)$ (squares) in a harmonic potential at $U = 3$, obtained from BD simulations.

The transition path time reads

$$\tau^{TP}(L|0) = \frac{L^2 \int_0^{\sqrt{U}} dy y^2 e^{-y^2} F_{2,2}(y^2)}{D\sqrt{\pi U} \text{erf}(\sqrt{U})}. \quad (101)$$

For small U we find the asymptotic expression

$$\tau^{TP}(L|0) D/L^2 \approx \frac{1}{6} - \frac{U}{90} - \frac{2U^2}{945}, \quad (102)$$

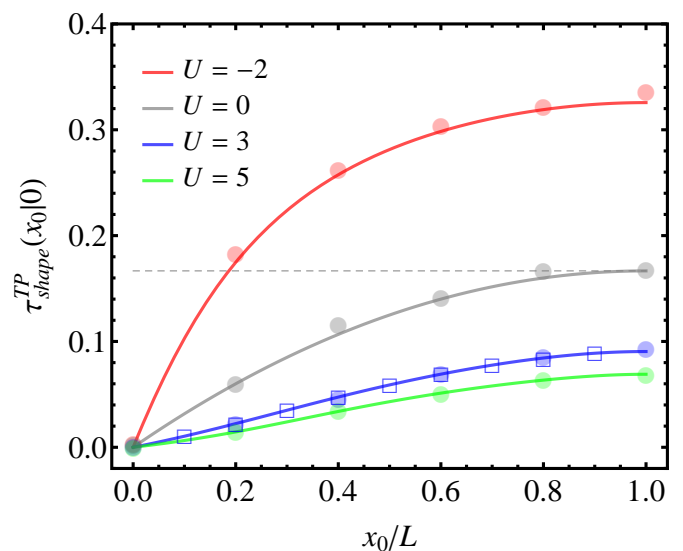


FIG. 7: Mean transition path shape $\tau_{shape}^{TP}(x_0|0)$ from Eq. (100), for different values of the barrier height U of the harmonic potential $F = 4Ux(1-x/L)/L$. Symbols show BD simulation results for $\tau^{FP}(0|x_0)$ (filled circles) and $\tau_{shape}^{TP}(x_0|0)$ (open squares) for $U = 3$. The horizontal dashed line depicts the force-free transition path time $\tau^{TP} = L^2/(6D)$.

while for large U we find

$$\tau^{TP}(L|0) D/L^2 \approx \frac{\ln U}{4U}. \quad (103)$$

Figure 8 depicts $\tau^{TP}(L|0)$ as function of the barrier height U . In Fig. 8(a) we show, on double logarithmic scales, the numerically integrated $\tau^{TP}(L|0)$ from Eq.

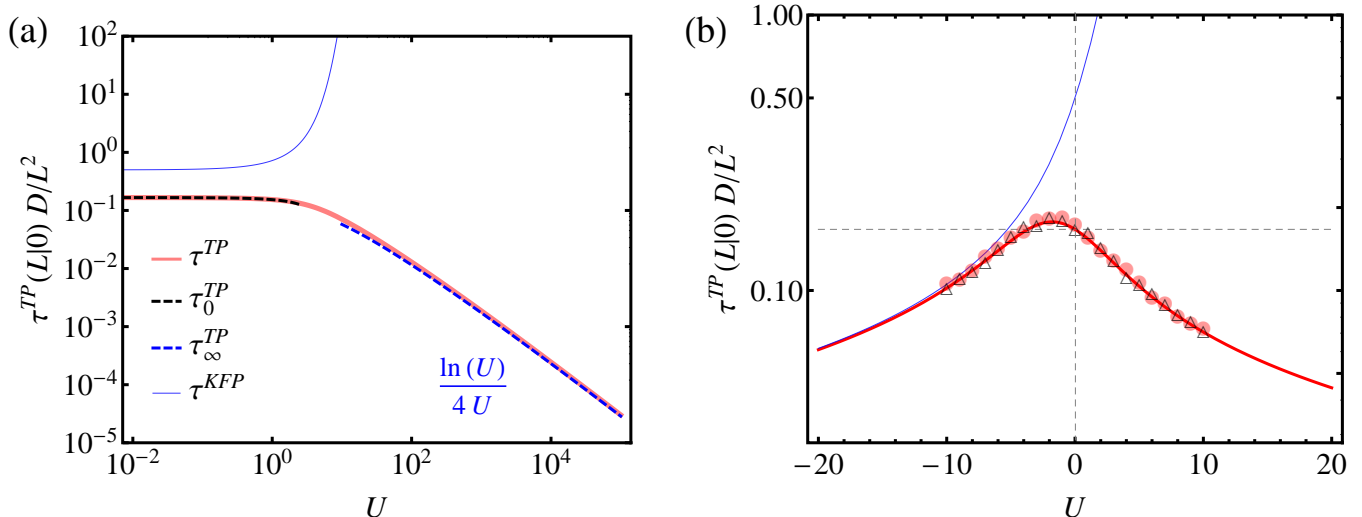


FIG. 8: Results for the harmonic ramp $F(x) = Ux(2-x/L)/L$. (a) Mean transition path time $\tau^{TP}(L|0)$ from Eq. (101) (solid red curve) on log-log scales, the asymptotic expressions Eqs. (102) and (103) are shown by dashed black lines. The blue line shows Kramers' mean first-passage time $\tau^{KFP}(L|0)D/L^2$ from Eq. (104). (b) Same curves shown on log-linear scales, compared with BD simulation data for transition paths starting from the left, $\tau^{TP}(L|0)$, (circles) and for transition paths starting from the right, $\tau^{TP}(0|L)$, (triangles). The horizontal dashed line depicts the force-free transition path time $\tau^{TP}(L|0)D/L^2 = 1/6$.

(101) by the solid red curve and compare with the asymptotic expressions Eqs. (102) and (103) (dashed curves). In Fig. 8-(b) we show $\tau^{TP}(L|0)$ from Eq. (101) on a log-linear scale, the symbols show BD simulation results. The solid blue curves in Fig. 8 depict the Kramers' mean first-passage time, which is given by

$$\tau^{KFP}(L|0) = \frac{L^2}{D} \left[\frac{\pi \operatorname{erf}(\sqrt{U}) \operatorname{erfi}(\sqrt{U})}{4U} - \frac{F_{2,2}(-U)}{2} \right], \quad (104)$$

and has the leading order expression

$$\tau^{KFP}(L|0) = \frac{\sqrt{\pi}L^2}{4D} \frac{e^U}{U^{3/2}}, \quad (105)$$

for large U .

The transition path time $\tau^{TP}(L|0)D/L^2$ is nonmonotonic and is maximal for finite U around $U \approx -21/8$, implying that transition paths that move down a weak harmonic ramp are slower than in the force-free case. For large $|U|$, $\tau^{TP}(L|0)$ decreases, similar to the linear potential case shown in Fig. 4-(a). In contrast, the Kramers' mean first-passage time $\tau^{KFP}(L|0)$ exponentially increases as U increases.

For the transition path shapes we find

$$\tau_{shape}^{TP}(x_0|0) = \tau^{TP}(L|0) - \frac{\sqrt{\pi}L^2}{2DU} \int_0^{y_0} dy e^{y^2} \operatorname{erf}(y) \left[1 + \frac{\operatorname{erf}(y)}{\operatorname{erf}(y_0)} - 2 \frac{\operatorname{erf}(y)}{\operatorname{erf}(\sqrt{U})} \right], \quad (106)$$

$$\tau_{shape}^{TP}(x_0|L) = \tau^{TP}(L|0) - \frac{\sqrt{\pi}L^2}{2DU} \int_{y_0}^{\sqrt{U}} dy e^{y^2} \frac{[\operatorname{erf}(\sqrt{U}) - \operatorname{erf}(y)] [\operatorname{erf}(y_0) - \operatorname{erf}(y)]}{\operatorname{erf}(y_0) - \operatorname{erf}(\sqrt{U})}, \quad (107)$$

where $y_0 \equiv \sqrt{U}(1-x_0/L)$.

Figure 9 depicts the transition path shapes starting from the left, $\tau_{shape}^{TP}(x_0|0)$ (solid curves) from Eq. (106), and starting from the right, $\tau_{shape}^{TP}(x_0|L)$ (broken curves)

from Eq. (107), for different values of the barrier height U . The symbols show the corresponding results from BD simulations. Note that the transition path shapes $\tau_{shape}^{TP}(x_0|0)$ and $\tau_{shape}^{TP}(x_0|L)$ at constant U are asym-

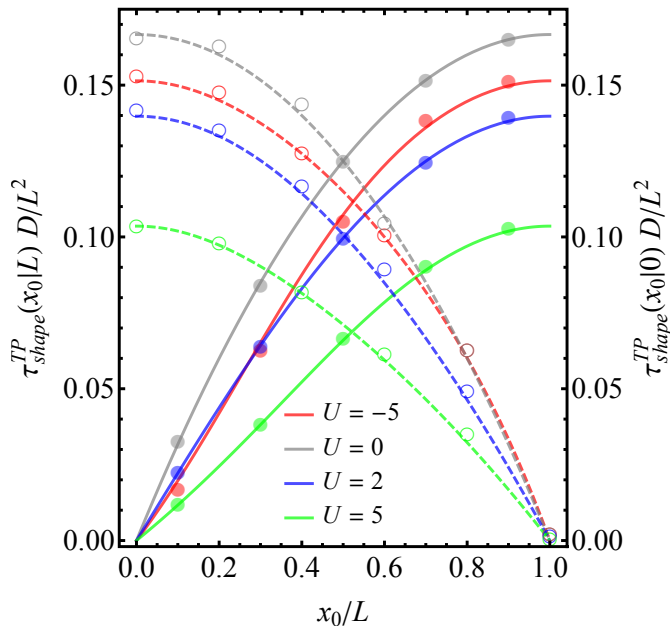


FIG. 9: Mean transition path shapes starting from the left, $\tau_{shape}^{TP}(x_0|0)$ (solid curves) from Eq. (106), and mean transition path shapes starting from the right, $\tau_{shape}^{TP}(x_0|L)$ (broken curves) from Eq. (107), for different values of the barrier height U of the harmonic ramp $F(x) = Ux(2-x/L)/L$. The symbols show the corresponding BD simulation results.

metric with respect to the exchange of starting and end positions, due to the asymmetry of the barrier potential (this becomes clear by comparing the mean shapes for $U = 0$ (grey line) and for $U = -5$ (red line) starting from the left boundary and starting from the right boundary).

V. CONCLUSION

Based on the one-dimensional Fokker-Planck equation, we develop the theoretical formalism to calculate mean shapes of transition paths and of Kramers' first-passage

paths for arbitrary free energy and diffusivity landscapes. We use a combination of the backward and forward Fokker Planck approaches to derive explicit expressions for transition and first-passage path shapes. To clarify the interpretation of our results, we also present convolution expressions for the distribution functions of transition path and passage times. We show that the mean shape of Kramers' first-passage paths is identical to the shape of transition paths shifted by a constant. Based on our analytic theory, we present mean shapes for several simple model potentials. We illustrate our results by trajectories generated from Brownian dynamics simulations. Interestingly, transition path shapes are intrinsically asymmetric, they start out with finite velocity and reach the target position with infinite velocity, which is easily understood from our sum rules for transition path and passage times.

The transition path shapes we predict can be compared straightforwardly with simulations for proteins that undergo folding and unfolding events and will allow for a crucial test of the assumptions underlying the projection onto a one-dimensional reaction coordinate. With further developments of experimental single-molecule techniques, our results for the transition path shapes can also be compared with experimental results in the future. For such a comparison, note that a reflecting boundary condition at $x = x_A$, as used in our calculations, is typically not present in molecular dynamics simulations nor in experiments. To apply our formulas, one can easily shift the reflecting boundary conditions to a position where the trajectory never visits. Alternatively, one can cut out all trajectory sections that visit the region behind the reflecting boundary condition and merge the remaining trajectory parts with a continuous concatenated time, which is valid in the limit of vanishing memory and effective mass.

Acknowledgements

The authors thank Bill Eaton for stimulating discussions. Financial support from the DFG (SFB 1078) is acknowledged.

-
- [1] P. G. Bolhuis, D. Chandler, C. Dellago, and P. L. Geissler, *Annu. Rev. Phys. Chem.* **53**, 291 (2002),
 - [2] R. B. Best and G. Hummer, *Proc. Natl. Acad. Sci. U.S.A.* **102**, 6732 (2005),
 - [3] P. Metzner, C. Schütte, and E. Vanden-Eijnden, *J. Chem. Phys.* **125**, 084110 (2006),
 - [4] G. Hummer, *J. Chem. Phys.* **120**, 516 (2004),
 - [5] S. Chaudhury and D. E. Makarov, *J. Chem. Phys.* **133**, 034118 (2010),
 - [6] E. Rhoades, M. Cohen, B. Schuler, and G. Haran, *J. Am. Chem. Soc.* **126**, 14686 (2004).
 - [7] H. S. Chung, J. M. Louis, and W. A. Eaton, *Proc. Natl. Acad. Sci. U.S.A.* **106**, 11837 (2009),
 - [8] H. S. Chung, K. McHale, J. M. Louis, and W. A. Eaton, *Science* **335**, 981 (2012),
 - [9] H. Yu, A. N. Gupta, X. Liu, K. Neupane, A. M. Brigley, I. Sosova, and M. T. Woodside, *Proc. Natl. Acad. Sci. U.S.A.* **109**, 14452 (2012),
 - [10] H. S. Chung and W. A. Eaton, *Nature* **502**, 685 (2013).
 - [11] T.-H. Lee, L. J. Lapidus, W. Zhao, K. J. Travers, D. Herschlag, and S. Chu, *Biophys. J.* **92**, 3275 (2007).
 - [12] K. Neupane, D. B. Ritchie, H. Yu, D. A. N. Foster, F. Wang, and M. T. Woodside, *Phys. Rev. Lett.* **109**, 068102 (2012),

- [13] K. Truex, H. S. Chung, J. M. Louis, and W. A. Eaton, *Phys. Rev. Lett.* **115**, 018101 (2015),
- [14] D. E. Shaw, P. Maragakis, K. Lindorff-Larsen, S. Piana, R. O. Dror, M. P. Eastwood, J. A. Bank, J. M. Jumper, J. K. Salmon, Y. Shan, W. Wriggers, *Science* **330**, 341 (2010).
- [15] Z. Zhang and H. S. Chan, *Proc. Natl. Acad. Sci. U.S.A.* **109**, 20919 (2012),
- [16] R. Frederickx, T. in't Veld, E. Carlon, *Phys. Rev. Lett.* **112**, 198102 (2014).
- [17] M. Sega, P. Faccioli, F. Pederiva, G. Garberoglio, and H. Orland, *Phys. Rev. Lett.* **99**, 118102 (2007),
- [18] H. Orland, *J. Chem. Phys.* **134**, 174114 (2011),
- [19] G. H. Weiss, *Adv. Chem. Phys.* **13**, 1 (1967).
- [20] A. Szabo, K. Schulten, and Z. Schulten, *J. Chem. Phys.* **72**, 4350 (1980),
- [21] R. Zwanzig, *Nonequilibrium Statistical Mechanics* (Oxford University Press, USA, 2001),
- [22] M. Hinczewski, Y. von Hansen, J. Dzubiella, and R. R. Netz, *J. Chem. Phys.* **132**, 245103 (2010),
- [23] Y. von Hansen, F. Sedlmeier, M. Hinczewski, and R. R. Netz, *Phys. Rev. E* **84**, 051501 (2011).
- [24] D. R. Cox, *Renewal theory*, vol. 4 (Methuen London, 1962).
- [25] N. G. Van Kampen, *Stochastic processes in physics and chemistry*, vol. 1 (Elsevier, 1992).
- [26] C. W. Gardiner, *Handbook of stochastic methods*, vol. 4 (Springer Berlin, 1985).